Mechanism of Solid/Liquid Interfacial Reactions. The Maleic Acid Driven Dissolution of Calcite: An Atomic Force Microscopy Study under Defined Hydrodynamic Conditions

Qi Hong, Marco Fidel Suárez, Barry A. Coles, and Richard G. Compton*

Physical and Theoretical Chemistry Laboratory, Oxford University, South Parks Road, Oxford OX1 3QZ, United Kingdom

Received: March 20, 1997; In Final Form: April 24, 1997[⊗]

The dissolution of calcite ($CaCO_3$) in the presence of aqueous solutions containing maleic acid (*cis*-HOOC−CH═CH−COOH) in the pH range 4.3−8.2 has been studied by means of atomic force microscopy utilizing a flow cell of known hydrodynamics and modelable convection/diffusion. The latter permits the interpretation of dissolution rate data as measured by the *z*-piezo voltage in terms of a mechanism involving concentrations of solution species *local* to the dissolving crystal surface. In this way the dissolution mechanism for the $(10\bar{1}4)$ cleavage plane is shown to proceed via reaction of the adsorbed monoprotonated anion, *cis*-HOOC−CH═CH−COO^-, but to be inhibited by the adsorbed dianion, $^-$OOC−CH═CH−COO^-. Where available excellent quantitative agreement is noted with independent surface averaged kinetic data previously (*J. Chem. Soc., Faraday Trans. 1* **1989**, *85*, 4335) obtained using a channel flow cell.

Introduction

The fundamental study of reactions between solids and liquid phase species is a subject of rapidly growing attention.[1,2] A variety of methods are emerging for kinetic and mechanistic studies, including hydrodynamic (for example rotating disc) methods, scanning electrochemical microscopy (SECM), and atomic force microscopy (AFM). The relative merits of these different techniques have been recently assessed in an admirable review.[2] AFM is able to image reacting or dissolving surfaces under liquid and can give spatially resolved kinetic information;[3−7] specifically by monitoring the evolution of suitable structural features in real time, such as the translation of steps across the surface, the rate of reaction/dissolution may be inferred and approximate estimations of the corresponding rates can be made. Alternatively a purely kinetic approach is to employ a channel flow cell[8−10] (CFC) to give rate data which, unlike AFM or SECM, is effectively averaged over the entire solid surface. However one merit of the CFC method is that the concentration of solution phase reactants near the solid surface is constantly refreshed by the flow, whereas in a stagnant medium there can be very considerable depletion of reactant, particularly in the case of reactive solids. Moreover if depletion does occur, then the deduction of interfacial mechanisms and associated rate laws is difficult as the concentrations local to the solid surface become unknown.

To overcome reactant depletion problems in atomic force microscopy, which has hitherto generally been used with either stagnant solution or ill-defined flow, we have developed[11] a novel flow cell, based on the standard Topometrix[12] Discoverer liquid immersion cell, in which AFM images may be obtained in the presence of a flowing liquid and in which the flow pattern may be calculated. The standard cell has tangential inlet and outlet ports at the periphery of a large irregular volume, so that the flow in the vicinity of the scanning cantilever is unpredictable. We have therefore redesigned the cell by the addition of a new inlet port so that solution can be delivered through a precisely shaped and positioned stainless steel duct directly to the front of the cantilever chip (Figure 1). The liquid jet is aligned parallel to the front of the cantilever support chip and transverse to the cantilever. This gives a free field flow, other than where confined by the sample below and the cantilever chip to one side. The resulting flow pattern is complex but can be solved[11] using computational fluid dynamics programs. In consequence, rates of interfacial reaction—as measured directly from the averaged imaged surface height via the *z*-piezo voltage—can be modeled in terms of reactant concentrations local to the surface as deduced via the appropriate convective−diffusion equations.[11]

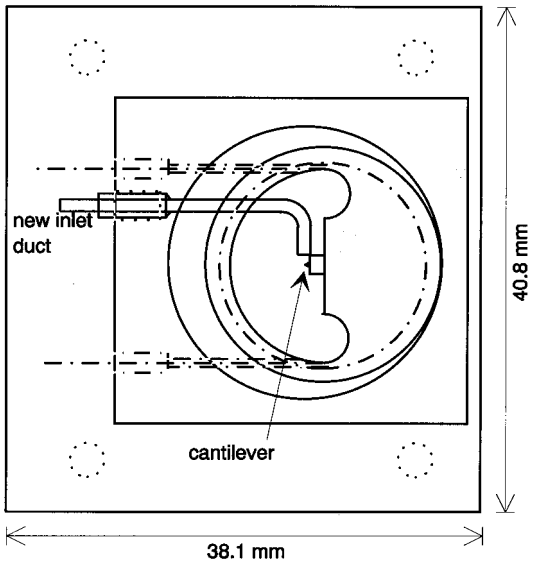

Figure 1. Top view of the Topometrix sample cell showing the new inlet duct.

In this paper we apply the hydrodynamic AFM flow cell to the study of the dissolution of calcite. This has major environmental, geological, and biological consequences. First the erosion of buildings, monuments and statues induced by acid rain raises serious conservation issues,[13−15] and second the ionic composition of sediments, soils, and marine and freshwater

[⊗] Abstract published in *Advance ACS Abstracts,* June 15, 1997.

S1089-5647(97)01011-0 CCC: $14.00

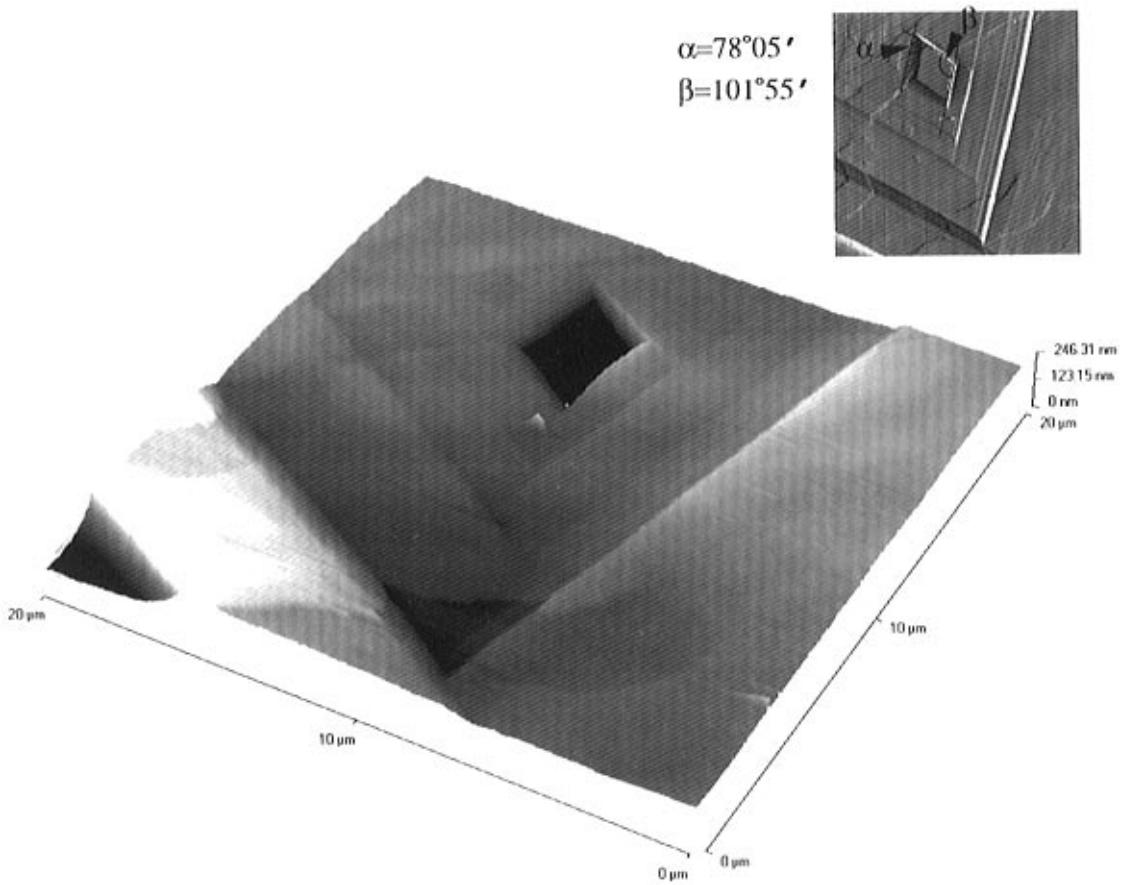

Figure 2. AFM image of a cleaved calcite crystal surface recorded under a flowing solution of pure water after exposure to a flow rate of 7.3×10^{-3} mL s^{-1} for 10 min.

systems is sensitive to calcite dissolution/precipitation processes,[16−20] which, third,[21−23] may also have medical implications. Usually below pH 5−6 and with mineral acids such as HCl, dissolution occurs primarily through direct reaction of aqueous protons at the $CaCO_3$ surface.[24−26] However in this paper we seek to explore the mechanism of dissolution as induced by an organic acid—maleic acid, H_2Mal—since in this case the adsorption of the corresponding dianion, Mal^{2-}, onto

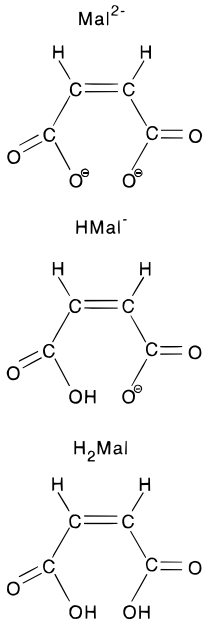

the calcite surface is believed, on the basis of channel flow cell data, to partially inhibit the dissolution reaction.[25]

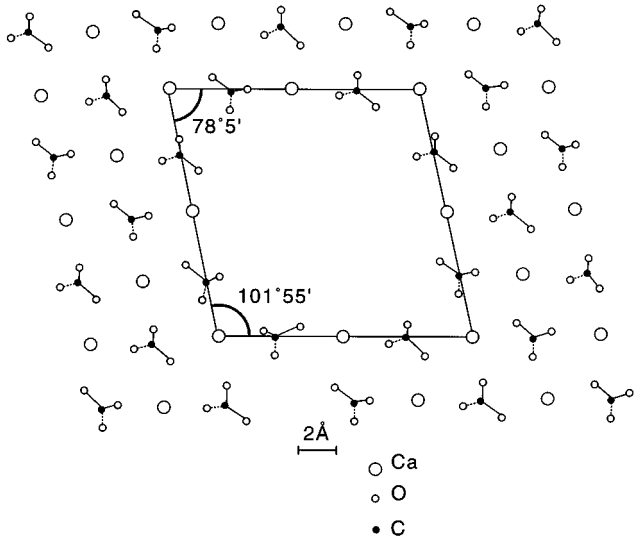

Figure 3. Diagram showing the calcite cleavage plane[30] and, schematically, the associated etch pits.

Experimental Section

A Topometrix TMX 2010 Discoverer atomic force microscope, operating in contact mode, was employed to image the surfaces of solid substrates. A commercial Topometrix liquid cell[12] was used, with modification[11] to allow for controlled and modelable hydrodynamics, for in situ AFM imaging. The rates of dissolution of the surfaces of single crystals of calcite were measured using the following procedure. First a single crystal was freshly cleaved and imaged in air, typically revealing a smooth (10$\bar{1}$4) surface with a few steps. Solution was then flowed through the liquid cell using a flow rate of 7.3×10^{-3} cm^3 s^{-1}, corresponding to a mean velocity of 1.9 cm s^{-1} in the

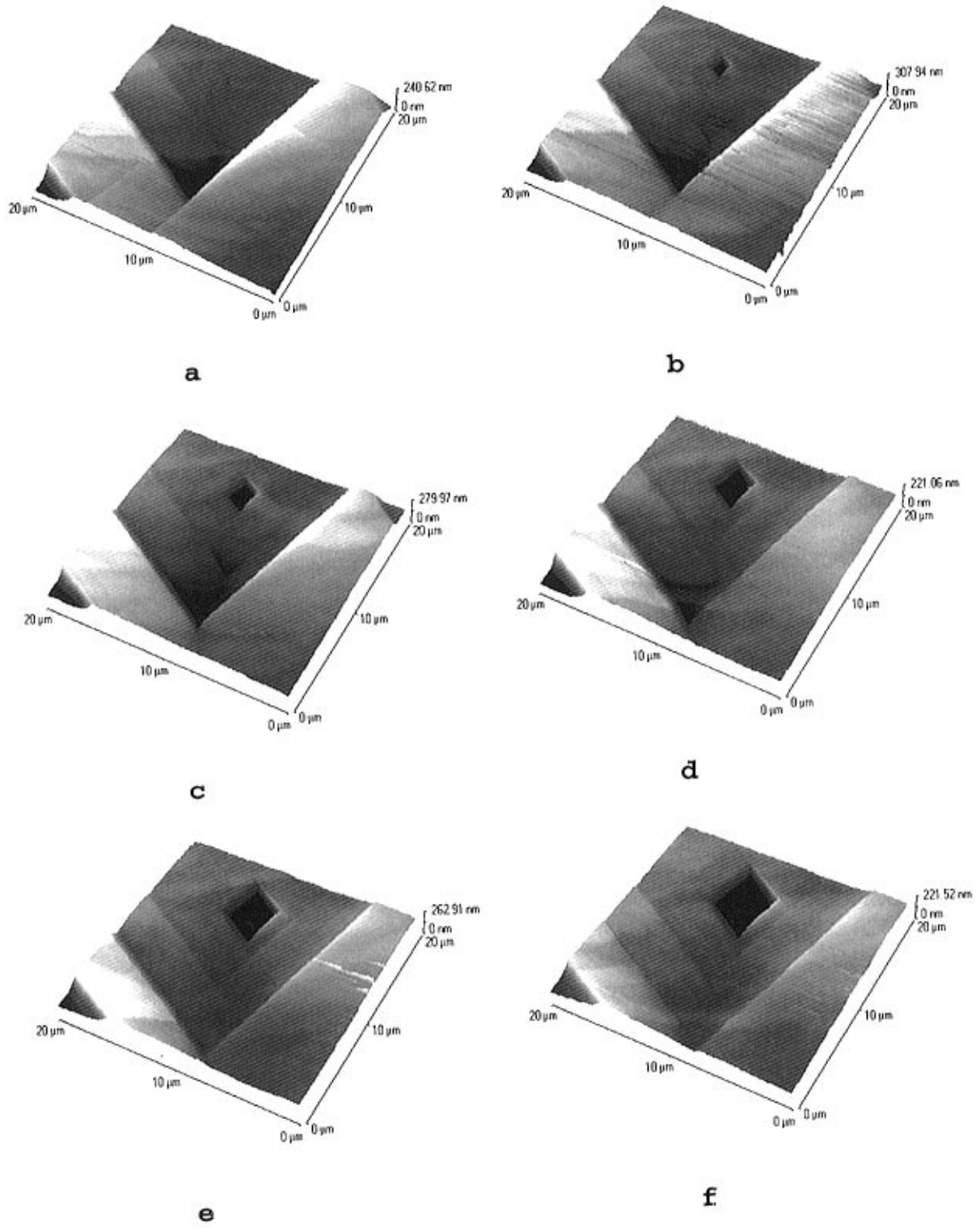

Figure 4. Sequence of six AFM images recorded under a flowing solution of nanopure water (7.3×10^{-3} mL s^{-1}) at times (a) 0, (b) 193, (c) 387, (d) 581, (e) 775, and (f) 969 s showing the evolution of an etch pit on the cleavage surface of calcite.

inlet duct and a solution shear rate of 125 s^{-1} at the cantilever location, and the same surface was then imaged in an aqueous environment. After slight initial dissolution and roughening of the surface in solution, several images were taken until any drift on the *x*- and *y*-piezo scanner elements was eliminated and their output steady. A series of images of the dissolving surfaces were then recorded continuously, at ca. 50 s intervals, corresponding to a scan rate of 10 Hz and a resolution of 200 × 200 data points per image. For quantitative experiments a scan area of 20 × 20 μm was employed. In all cases two sorts of experiment were undertaken: first, the recording of conventional topographical images and, second, the monitoring of the absolute *z*-piezo voltage during scanning. The latter was recorded by scaling down the *z*-piezo voltage using a potential divider and feeding it to an external input channel of the electronic control unit of the AFM, which permitted an absolute voltage map of the scanned area to be generated. Calibration of the voltage then permitted real drops or increases in height to be measured. This calibration was achieved by imaging a test grid, with a known precisely defined thickness of 2400 Å, and measuring the *z*-piezo voltage changes between topographical maxima and minima. Using this procedure, a voltage-height "conversion constant" of 0.308 V/μm was calculated. In this way the height of the crystal could be measured throughout the dissolution

period in the presence of a flowing solution of aqueous acid. Measurements were under ambient temperature conditions of 20 ± 1 °C.

Solutions were made up using triply distilled deionized water of resistivity > 10^7 Ω cm (from an Elgastat system, High Wycombe, U.K.) and, where possible, AnalaR grade reagents ($Ca(NO_3)_2$, Na_2CO_3, NaOH, all Aldrich). Buffer solutions for pH 9 contained either 0.0125 M borax and 0.0046 M HCl Aldrich) or TRIZMA, 0.5 M tris(hydroxyl)aminomethane (Fluka), adjusted to the required pH by the addition of volumetric standard HCl (Aldrich). Disodium maleate (Sigma) was used to prepare a concentration sequence between 0 and 1.2×10^{-2} M and modified to pH 5 with volumetric standard HCl. A pH sequence between 4.2 and 8.9 with a total concentration of 5 mM in Mal^{2-}/$HMal^-$ was prepared by changing the ratio of disodium and monosodium maleate (Sigma). Argon, used to degas the solutions, was supplied by the British Oxygen Co. Thin slices of calcite crystals were cleaved using a clean heavy-duty blade from a block of semioptical quality Iceland Spar which originated in Chihuahua, Mexico (supplied by Richard Tayler Minerals, Cobham, Surrey, U.K.), and previously characterized.[24] All AFM imaging was performed on the rhombohedral cleavage plane ($10\bar{1}4$).

Results and Discussion

Initial experiments were conducted in the absence of maleic acid, or its salts, to permit comparison with previous reports.[3,27,28] The ($10\bar{1}4$) cleavage plane was imaged under flow using the modified AFM liquid cell.[11] Exposure to nano-pure water was found to induce the formation of rhombic-shaped etch pits on the calcite surface (Figure 2) with internal angles of 101° 55′ and 78° 05′, corresponding to the unit cell exposed in the cleavage plane of the calcite crystal[30] (Figure 3). Sequences of images were recorded in real time; Figure 4 shows a representative set of six consecutive scans which clearly show the nucleation and growth of an etch pit. Examination of such sequences permits the estimation of the mean linear rate of pit growth into the adjacent cleavage terrace as 5.0 ± 0.2 nm s^{-1}. This value compares favorably with that obtained via optical microscopy[27] (5.4 nm s^{-1}) and through AFM[28] (4.9 nm s^{-1}) both at pH 9.

Next, medium effects on the high pH (>5−6) dissolution process were examined. Experiments with two different buffer solutions at pH 9—borax and TRIZMA—using a flow rate of 7.3×10^{-3} mL s^{-1} showed etch pits comparable to those observed for pure water (Figure 4). These grew with linear rates similar to those observed in the absence of buffer. Next, separate experiments were conducted with solutions containing 10^{-3} M $Ca(NO_3)_2$, 10^{-4} M $Ca(NO_3)_2$, or 10^{-3} M Na_2CO_3. In all three cases the formation of etch pits was suppressed, but if pure water was subsequently flowed into the cell, pits immediately grew at the rate expected for pure water for the case of both $Ca(NO_3)_2$ solutions but only after a period of ca. 120 min for Na_2CO_3. These qualitative observations clearly point to the effects of surface adsorbed ions in controlling the dissolution processes via growing etch pits. Moreover the slowness of recovery from exposure to carbonate-containing solutions is consistent with the previously inferred stronger adsorption of CO_3^{2-} as compared to Ca^{2+} on calcite.[30,31] The literature[25] suggests that a profitable system for the *quantitative* study of surface adsorption effects on $CaCO_3$ dissolution is in the context of the proton-induced calcite dissolution in the presence of maleic acid. It is to this problem that we next turn.

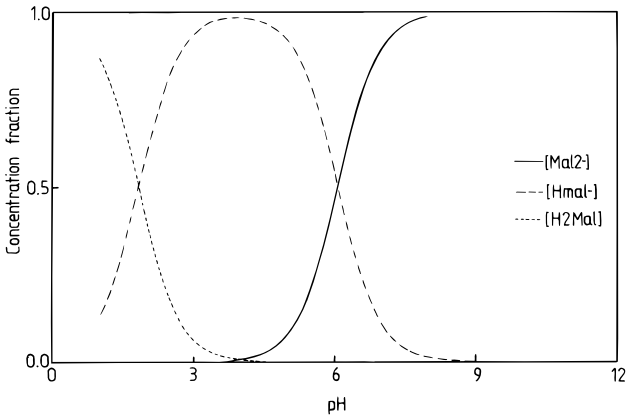

Figure 5. Relative speciation of a solution containing H_2Mal, $HMal^-$, and Mal^{2-} as a function of pH.

In situ AFM studies were first conducted on the dissolution of calcite in aqueous solutions containing a total of 5 mM Mal^{2-} and $HMal^-$ over a range of pH values between 4.3 and 8.2. The relative amounts of the two ions present as a function of pH are shown in Figure 5 calculated assuming values of 1.83 and 6.07 for the pK_a values of the two H_2Mal protons.[32] Clearly at the lower pH values studied the composition is predominantly $HMal^-$, while at the higher pH values Mal^{2-} is the majority species. Figure 6 shows representative pit shapes obtained at different pH values. At the lowest pH studied oval etch pits are observed, as has been reported on the basis of optical measurements[26] and interpreted in terms of the adsorption of the Mal^{2-} ion by the pairs of Ca^{2+} ions that bridge across the narrow angle of the unit cell in the cleavage plane (Figure 7). As the pH increases, the etch pits gradually change to a hexagonal shape, and by pH 8.2 the shape has again changed to resemble those seen in pure water. The orientation of the oval and hexagonal pits to the unit cell of the cleavage plane is shown in Figure 7.[26]

For all (bulk) pH's studied it was possible to measure the rate of growth of the pits both in the direction of the relatively uninhibited dissolution (along the long axis of the oval pits, or parallel to the axis joining the two wide angles of the unit cell; see Figure 7) and in a direction at right angles to this in the direction of the relatively most inhibited dissolution (along the short axis of the oval pits, or parallel to the axis joining the two narrow angles of the unit cell). In all cases the rate of growth was found to be closely constant with time but to be (bulk) pH dependent, as shown in Figure 8. In parallel with these kinetic observations on individual pits, measurements were also made of the average *z*-piezo voltage applied (see the Experimental Section) throughout a prolonged dissolution period of 15 min. This was found to vary linearly with time, permitting the mean (surface-averaged) dissolution rate to be found as a function of pH; this is shown in Figure 9. The broad decrease with pH in Figures 8 and 9 is clearly related to the reduction of $[H^+]$ and, particularly, $[HMal^-]$ with increasing pH. We return to the quantitative interpretation of these plots below.

Studies were also carried out under flowing conditions at a fixed pH of 5 but with varying amounts of total dissolved maleate in the range 0−12 mM. Figure 10 shows that the oval pit shape is highly sensitive to the levels of dissolved maleate, changing from the shape of the unit cell at low maleate levels to oval shaped at higher concentrations. Moreover the ratio of the long to short axis of the oval pits first becomes greater with enhanced quantities of maleate but then passes through a maximum near 7 mM and then decreases! The variation of the absolute rate of growth is shown in Figure 11; note the

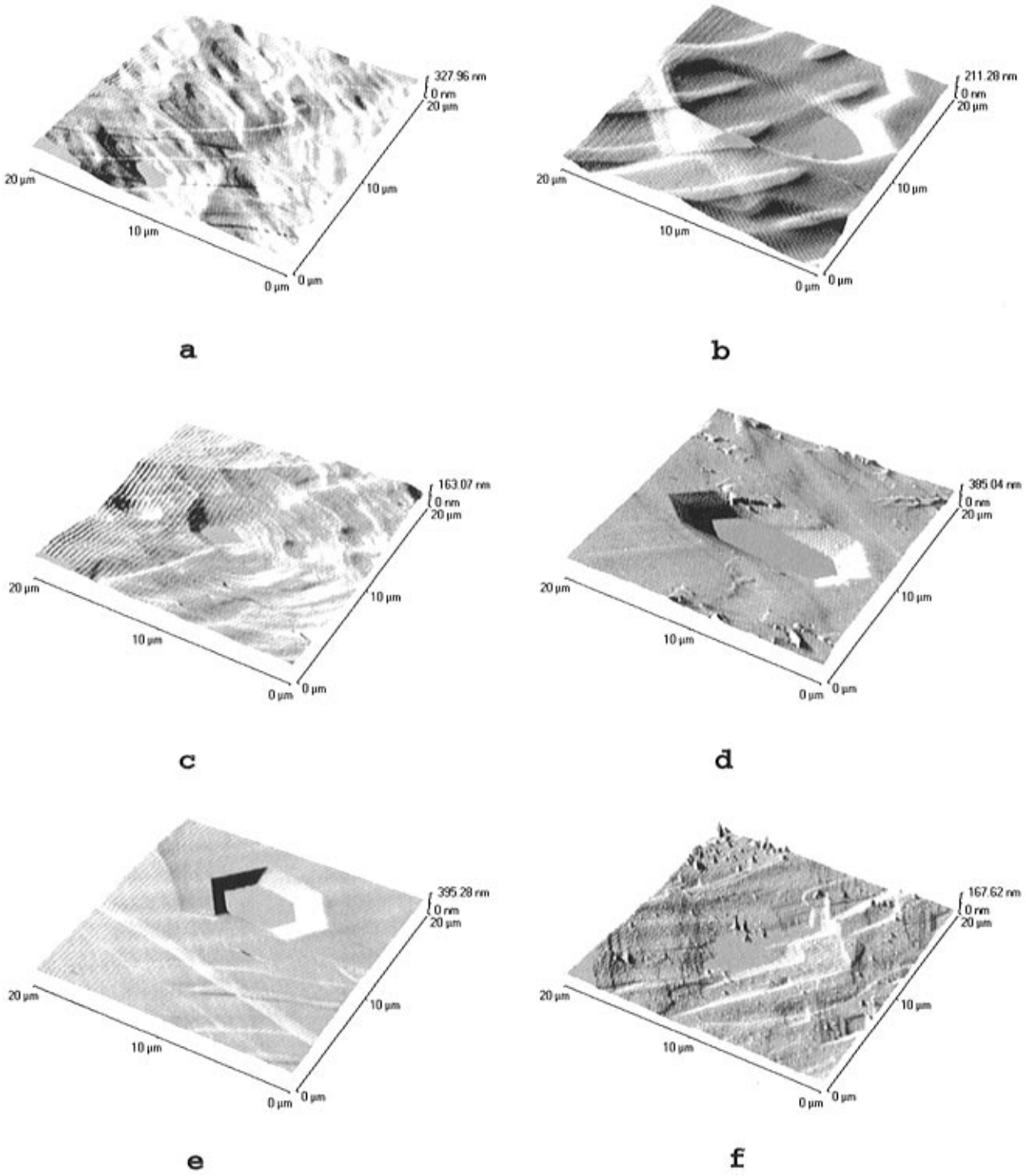

Figure 6. Images showing the contrasting etch pit shapes formed at different pH's: (a) 4.31, (b) 5.83, (c) 6.18, (d) 6.53, (e) 7.01, and (f) 8.19. All measurements were made under flowing conditions (7.3×10^{-3} mL s^{-1}) using a solution containing 5 mM $HMal^- + Mal^{2-}$.

abscissa shows bulk [$HMal^-$], not the total maleate concentration. The data presented in Figure 11 were obtained by monitoring the pit size over a typical period of 250 s, as illustrated in Figure 12. Also it was again possible to monitor via the *z*-piezo voltage large areas of the dissolving surface over periods of time up to 15 min so as to establish surface-averaged dissolution rates. Figure 13 shows how this rate varies with [$HMal^-$]; again an initial increase up to a maximum is evident, followed by a decrease.

We consider next the quantitative interpretation of the data given above and note that Unwin et al.[25] have, on the basis of surface-averaged kinetic measurements at channel flow cells, proposed that, where [H_2Mal] is negligible and [H^+] << [$HMal^-$] the dissolution is driven by the monoprotonated form of maleic acid:

$$HMal(aq) + CaCO_3(s) \rightarrow Ca^{2+}(aq) + HCO_3^-(aq) + Mal^{2-}(aq)$$

$$Mal^{2-}(aq) \rightleftharpoons Mal^{2-}(ads)$$

with a flux given by

$$j = k'[HMal^-]_0(1 - \theta_{Mal2-}) \quad (1)$$

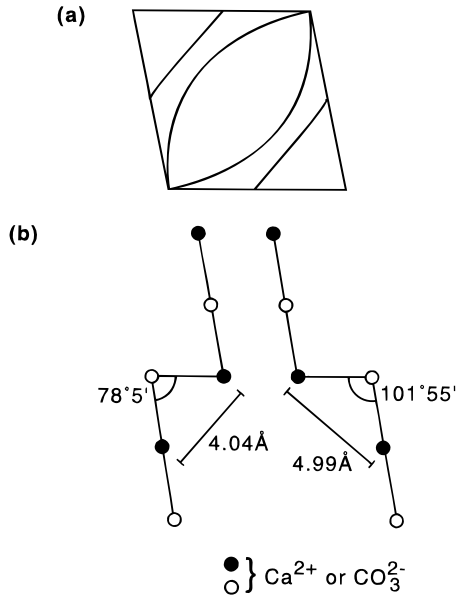

Figure 7. (a) Orientation of etch pits within the calcite cleavage plane. (b) Two different kink sites which can be formed on the ($I0\bar{I}4$) plane.

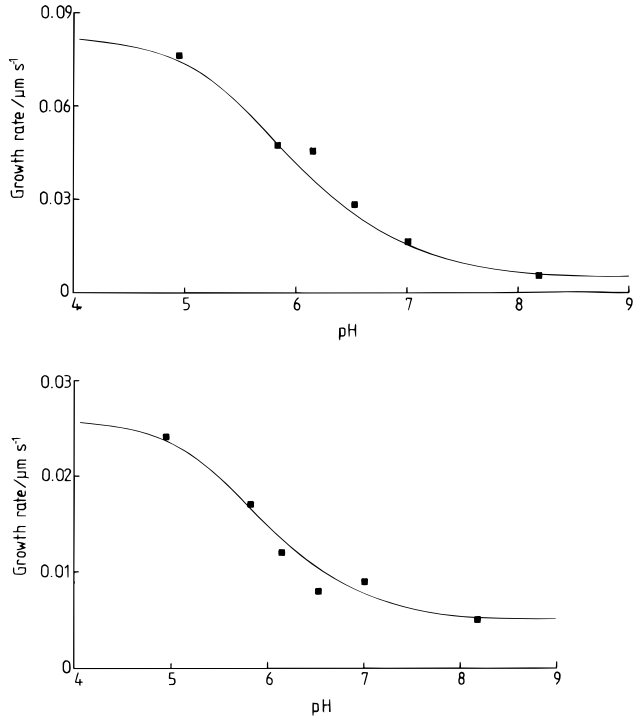

Figure 8. Rate of growth (μm s^{-1}) of etch pit (a) length and (b) width as a function of pH (flow rate 7.3 mL s^{-1}). The solid lines depict, in each case, the theoretical model described in the text.

where $[HMal^-]_0$ is the concentration of the monoanion *in the solution adjacent to the surface of the calcite crystal*, k'/cm s^{-1} is a rate constant, and θ_{Mal2-} denotes the (average) surface coverage of the maleic acid dianion. The latter was assumed to be Langmuirian:[25]

$$\theta_{Mal2-} = K_2[Mal^{2-}]_0/(1 + K_2[Mal^{2-}]_0) \qquad (2)$$

Since the data shown in Figures 8, 9, 11, and 13 were all collected under conditions of well-defined hydrodynamic flow, it was possible to test the model implied by eqs 1 and 2 using

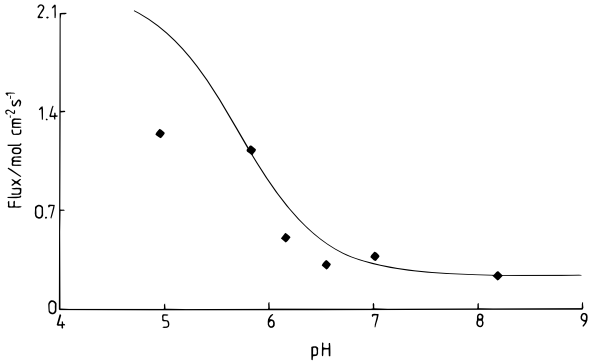

Figure 9. Surface-averaged rate of dissolution of the calcite cleavage plane measured at a flow rate of 7.3×10^{-3} mL s^{-1} as a function of pH. The rate was deduced directly from measurements of the mean *z*-piezo voltage as a function of time together with the known density of calcite.[33]

the values for k' and K_2 reported from channel flow cell measurements[25] (0.043 cm s^{-1} and 4.8×10^3 dm^3 mol^{-1}). This modeling was implemented as described in ref 11 so as to allow for the reduction in $[HMal^-]$ near the reactive surface and, similarly, the enhanced local concentration of Mal^{2-}. Note that the model had *no* adjustable parameters since the flow profile of the AFM hydrodynamic cell was established independently[11] and the relevant diffusion coefficients, rate constants, and equilibrium constants were all known from CFC studies.[25] The results of this modeling exercise are shown in Figure 13. It can be seen that remarkably good agreement between theory and experiment is seen at low concentrations of maleate where there is *quantitative* agreeement between the CFC data and that measured directly using atomic force microscopy through the *z*-piezo technique. The degree of correlation observed lends strong support to the hydrodynamic and convective−diffusion models developed in respect of the hydrodynamic AFM cell.

Returning to Figure 13, it can be seen that at high maleate levels theory and experiment deviate and, in particular, the former is unable to predict the maximum seen in the experimental data. An analogous maximum is present in both plots in Figure 11, and it is evident that eqs 1 and 2 are unable to predict this behavior. Accordingly we develop the previous model[26] and speculate that the $HMal^-$-driven dissolution proceeds via prior adsorption of $HMal^-$:

$$HMal^-(aq) \rightleftharpoons HMal^-(ads) \qquad \text{(fast)}$$

$$HMal(ads) + CaCO_3(s) \rightarrow Ca^{2+}(aq) + HCO_3^-(aq) + Mal^{2-}(ads) \qquad \text{(slow)}$$

$$Mal^{2-}(aq) \rightleftharpoons Mal^{2-}(ads) \qquad \text{(fast)}$$

In this case we might expect the rate equation to become

$$j/\text{mol cm}^{-2}\text{ s}^{-1} = k''\theta_{HMal-}(1 - \theta_{Mal2-}) \qquad (3)$$

where we again assume the adsorption to be Langmuirian:[34]

$$\theta_{HMal-} = K_1[HMal^-]_0/(1 + K_1[HMal^-]_0) \qquad (4)$$

This rate law reduces to eq 1 at sufficiently low values of $[HMal^-]$ provided $k''K_1 = k'$.

The model implied by eqs 2, 3, and 4 was implemented in the context of the hydrodynamic AFM flow cell again assuming the literature parameters derived from CFC experiments[25] but

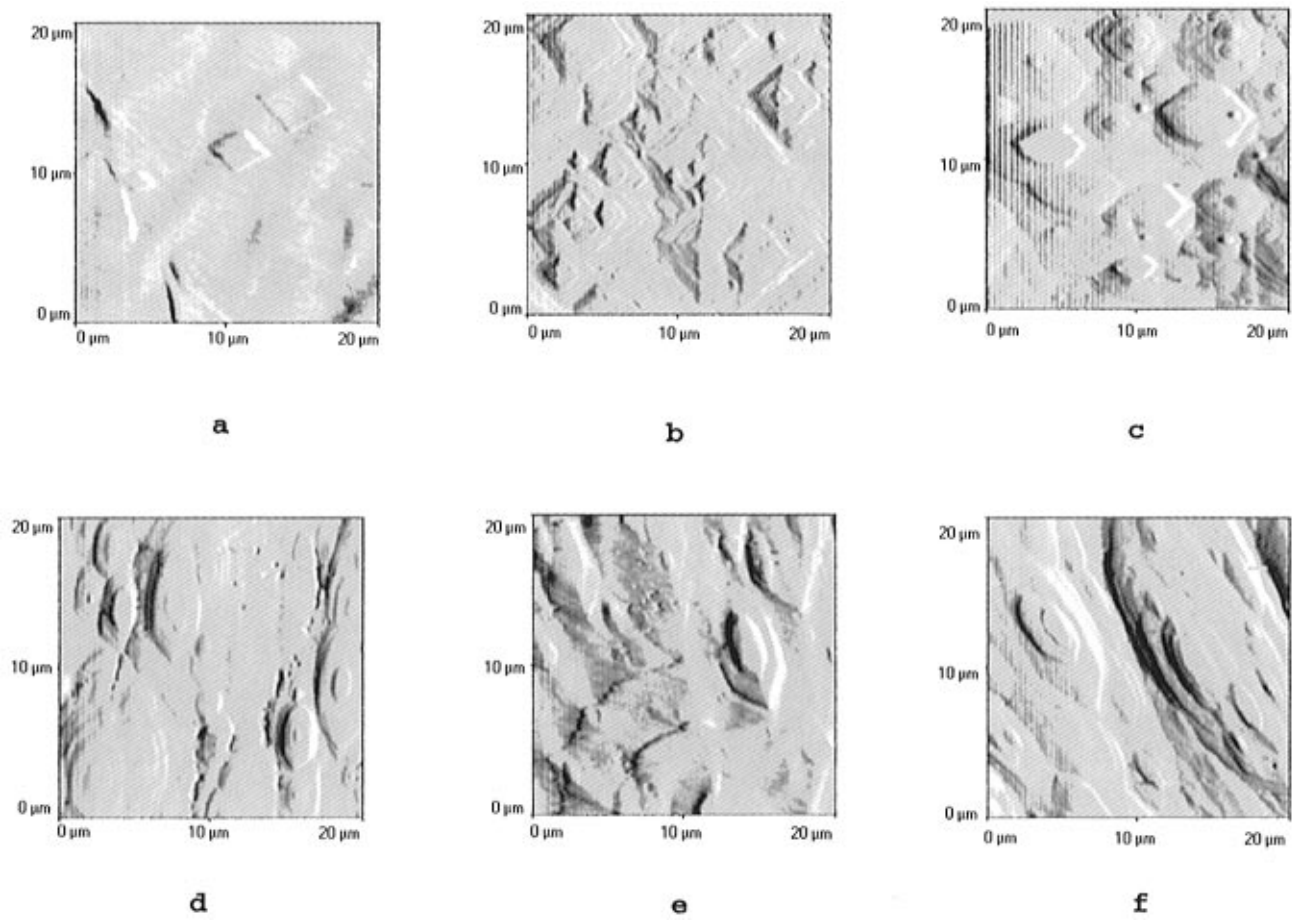

Figure 10. Images showing the contrasting etch pit shapes formed at different concentrations of total dissolved maleate: (a) 0.0, (b) 1.0, (c) 3.0, (d) 5.0, (e) 7.0, and (f) 9.0 mM. All measurements were made under flowing conditions (7.3×10^{-3} mL s^{-1}) using a solution of pH 5.

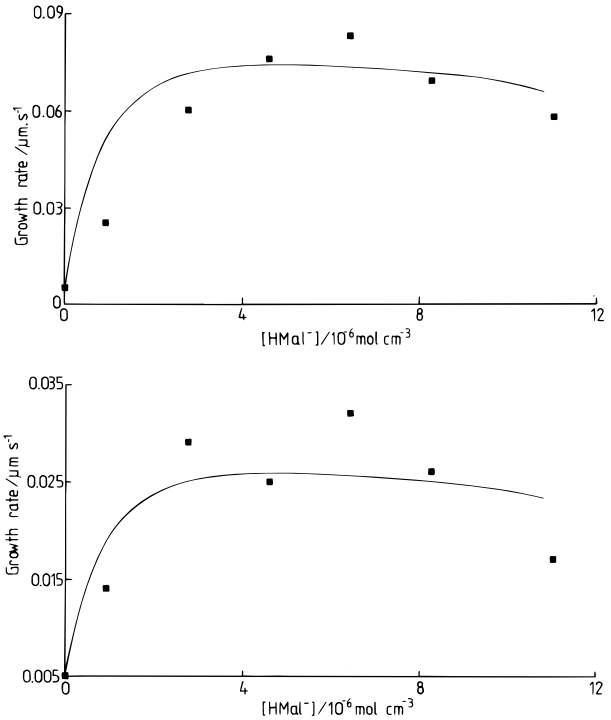

Figure 11. Rate of growth (μm s^{-1}) of (a) the length and (b) the width of the oval etch pits at pH 5 as a function of bulk [$HMal^-$] (flow rate 7.3×10^{-3} mL s^{-1}). The solid lines depict, in each case, the theoretical model described in the text.

treating the Langmuir adsorption constant, K_1, for the uptake of $HMal^-$ as an adjustable parameter. A value of 1.0×10^3 cm^3 mol^{-1} was found to fit *all* our experimental data: the solid lines shown in Figures 9 and 13 give the results of this modeling. Excellent agreement with the AFM data is observed, strongly supporting the kinetic model proposed above.

We now return to Figures 8 and 11, which quantify the rate of growth of etch pits on the calcite surface as a function of pH and [$HMal^-$], respectively. Application of the model derived above for the surface-averaged dissolution flux would predict the following equations for the velocity, v, of lateral movement of the pit into the adjacent ($I0\bar{I}4$) terrace:

$$v = v_0 + k^* \theta_{\mathrm{HMal-}}(1 - \theta_{\mathrm{Mal2-}}) \qquad (5)$$

where v_0 is the known growth velocity of the pit in the absence of maleic acid (5.0 nm s^{-1}) and k^* is a constant that depends on the direction of growth. Equation 5 was found to give a good fit to the experimental data, as shown in Figures 8 and 11, providing a value of 0.74 μm s^{-1} was chosen for dissolution in the direction of the long axis of the pit and a value of 0.20 μm s^{-1} for the short axis. The agreement between theory and experiment can be seen to be essentially quantitative, and this again supports the proposed dissolution mechanism.

Conclusions

The hydrodynamic AFM cell has been shown to permit the deduction of interfacial reaction mechanisms and to provide quantitative rate data that bears comparison with independent kinetic measurements.

Acknowledgment. We thank EPSRC for support via ROPA, the National Scholarship Council for International Studies of China, for support for Q.H. and COLIENCIAS for a scholarship for M.F.S.

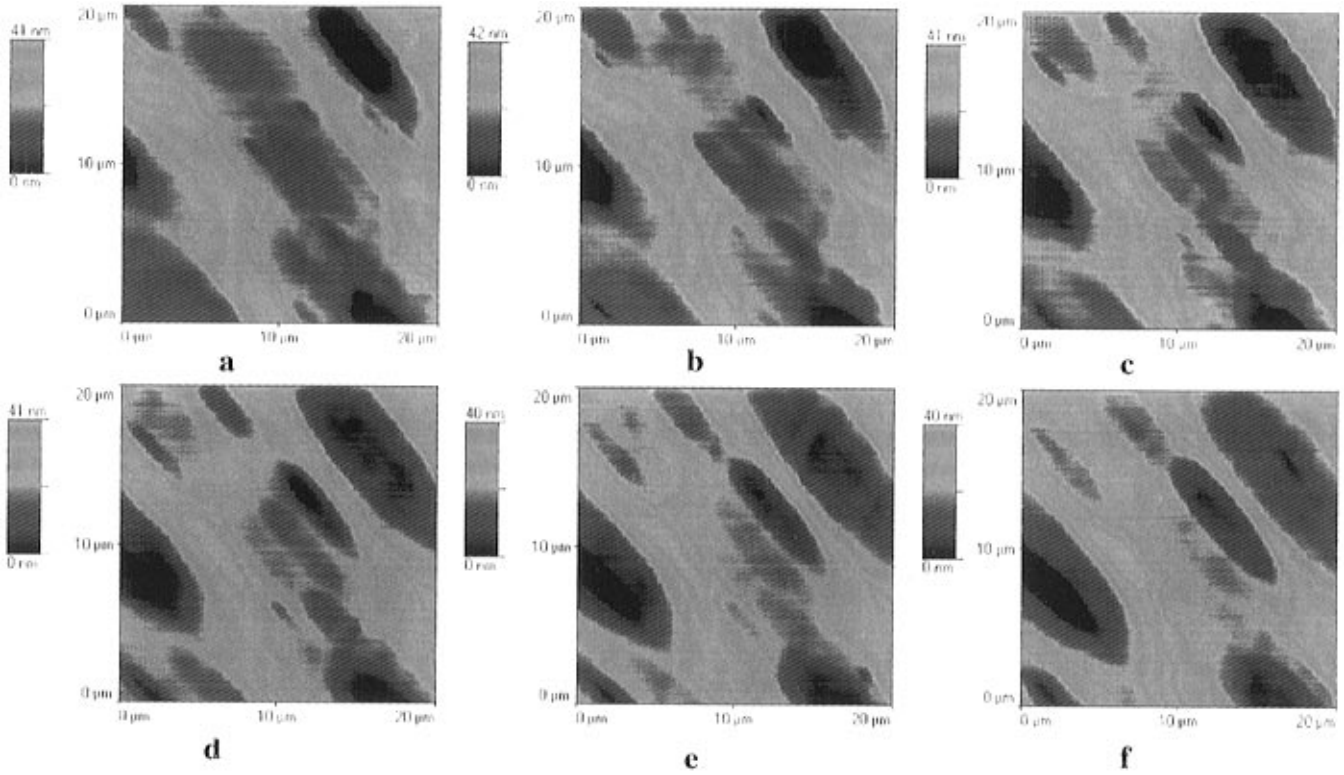

Figure 12. Sequence of six AFM images recorded under a flowing solution (9×10^{-3} mL s^{-1}) of pH 5 and containing a total maleate concentration of 5 mM at times (a) 0, (b) 50, (c) 100, (d) 150, (e) 200, and (f) 250 s showing the evolution of oval etch pits on the cleavage surface of calcite.

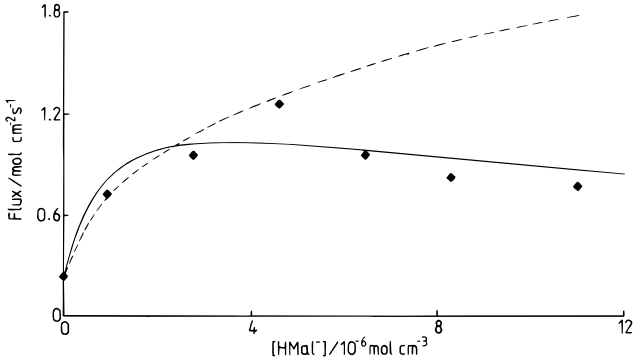

Figure 13. Surface-averaged rate of dissolution of the calcite surface measured as a function of [$HMal^-$] at pH 5 using a flow rate of 7.3×10^{-3} mL s^{-1}. The rate was deduced directly from measurements of the mean *z*-piezo voltage as a function of time together with the known density of calcite.[33] The solid line shows the prediction of the theoretical model described in the text. The dashed line shows the predictions of the simplified model based on ref 25.

References and Notes

(1) Atherton, J. H. *Res. Chem. Kinet.* **1996**, *2*, 193.
(2) Macpherson, J. V.; Unwin, P. R. *Prog. React. Kinet.* **1995**, *20*, 245.
(3) Hillner, P. E.; Manne, S.; Gratz, A. J. *Ultramicroscopy* **1992**, *42*−*44*, 1387.
(4) Hillner, P. E.; Manne, S.; Gratz, A. J. *Geology* **1992**, *20*, 359.
(5) Shakesheff, K. M.; Davies, M. C.; Domb, A.; Jackson, D. E.; Roberts, C. J.; Tendler, S. J. B.; Williams, P. M. *Macromolecules* **1995**, *28*, 1108.
(6) Chen, X.; Shakesheff, K. M.; Davies, M. C.; Heller, J.; Roberts, C. J.; Tendler, S. J. B.; Williams, P. M. *J. Phys.Chem.* **1995**, 99, 11537.
(7) Hall, C.; Cullen, D. C. *AICHE J.* **1996**, *42*, 232.
(8) Tam, K. Y.; Compton, R. G.; Atherton, J. H.; Brennan, C. M.; Docherty, R. *J. Am. Chem. Soc*. **1996**, *118*, 4419.
(9) Compton, R. G.; Harding, M. S.; Pluck, M. R.; Atherton, J. H.; Brennan, C. M. *J. Phys. Chem*. **1993**, *97*, 10416.
(10) Compton, R. G.; Harding, M. S.; Atherton, J. H.; Brennan, C. M. *J. Phys. Chem.* **1993**, *97*, 4677.
(11) Coles, B. A.; Compton, R. G.; Booth, J.; Hong, Q.; Sanders, G. H. W. *J. Chem. Soc., Chem. Commun.* **1997**, 619.
(12) Topometrix Corporation, Santa Clara, CA.
(13) Schiavon, N.; Ciavari, G.; Schiavon, G.; Fabbri, D. *Sci. Total Environ.* **1995**, *167*, 87.
(14) Elfving, P.; Panas, I.; Lindquist, O. *Appl. Surf. Sci*. **1994**, *78*, 83.
(15) Haneef, S. J.; Johnson, J. B.; Thompson, G. E.; Wood, G. C. *Corros. Sci*. **1993**, *34*, 497.
(16) Compton, R. G.; Pritchard, K. L.; Unwin, P. R. *Freshwater Biol*. **1989**, *22*, 285.
(17) Morse, J. W. *Marine Chem*. **1986**, *20*, 91.
(18) House, W. A. *Res. Chem. Kinet.* **1993**, *1*, 107.
(19) Orton, R.; Unwin, P. R. *J. Chem. Soc., Faraday Trans*. **1993**, *89*, 3947.
(20) Buhmann, D.; Dreybrodt, W. *Chem. Geol*. **1985**, *48*, 189.
(21) Walker, M. M.; Katz, J. L. *J. Dental Res*. **1984**, *63*, 325.
(22) Hay, D. I.; Schluckebier, S. K.; Moreno, E. C. *Calcif. Tissue Int*. **1986**, *39*, 151.
(23) Fujita, Y.; Yamamuro, T.; Nakamura, T.; Kotani, S.; Ohtsuki, C.; Kokubo, T. *J. Biomed. Mater. Res*. **1991**, *25*, 991.
(24) Compton, R. G.; Unwin, P. R. *Philos. Trans. R. Soc. London A* **1990**, *330*, 1.
(25) Compton, R. G.; Pritchard, K. L.; Unwin, P. R.; Grigg, G.; Silvester, S.; Lees, M.; House, W. A. *J. Chem. Soc., Faraday Trans. 1* **1989**, *85*, 4335.
(26) Barwise, A. J.; Compton, R. G.; Unwin, P. R. *J. Chem. Soc., Faraday Trans*. **1990**, *86*, 137.
(27) MacInnis, I. N.; Brantley, S. L. *Geochim. Cosmochim. Acta* **1992**, *56*, 1113.
(28) Liang, Y.; Baer, D. R.; McCoy, J. M.; Amonette, J. E.; LaFemina, J. P. *Geochim. Cosmochim. Acta* **1996**, *60*, 4883.
(29) Reeder, R. J. *Rev. Mineral.* **1983**, *11*, 1.
(30) Thompson, D. W.; Pownall, P. G. *J. Colloid Interface Sci.* **1989**, *131*, 74.
(31) Brown, C. A.; Compton, R. G.; Narramore, C. A. *J. Colloid Interface Sci.* **1993**, *160*, 372.
(32) Weast, R. C. *Handbook of Chemistry and Physics*; Chemical Rubber Co.: Boca Raton, FL, 1975.
(33) Lide, D. R. *Handbook of Chemistry and Physics*; Chemical Rubber Co.: Boca Raton, FL, 1993.
(34) Note that eq 4 implies the adsorption of $HMal^-$ is *not* competitive with that of Mal^{2-}, for which case the equation $\theta_{HMal^-} = K_1[HMal^-]_0/(1 + K_1[HMal^-]_0 + K_2[Mal^{2-}]_0)$ would apply. This possibility was considered but found to be quantitatively incompatible with our experimental data regardless of the value of K_1 chosen to model the data.